# In Operando Characterization of Li Composite Battery Electrode by Ellipsometry and Raman Spectroscopy. The Case of $Li_4Ti_5O_{12}$ Based Anode.

## エリプソメトリーとラマン分光法によるリチウム複合電極のオペランド解析 ～$Li_4Ti_5O_{12}$負極の場合～

Valerie SILLER
バレリー シラー

Alex MORATA
アレックス モラタ

Juan Carlos Gonzalez-ROSILLO
フアン カルロス ゴンサレス ロシリョ

Marc Nuñez EROLES
マルク ヌネス エロレス

Michel STCHAKOVSKY
ミッシェル スタコフスキー

Albert TARANCON
アルベルト タランコン

Lithium titanium oxide thin films are increasingly popular anode materials for applications in lithium-ion microbatteries and hybrid supercapacitors, due to their improved safety, cost and cycle lifetime. Nanoengineering of their stoichiometry and crystallinity can modify their lithium-site occupancy and stretch the materials specific capacity. So far, research efforts have mainly focused on the pure spinel phase $Li_4Ti_5O_{12}$ (LTO) and only a small fraction is dedicated to a broader spectrum of titanium-based metal oxide thin films. In this work, Pulsed Laser Deposition (PLD) is used by alternating LTO and $Li_2O$ ablations to create a wide landscape in the composition of titania-based micro-anodes. Their structures are studied by Raman Spectroscopy (RS) and their performances by In Operando Spectroscopic Ellipsometry (SE).

Key words
microbatteries, lithium titanium oxide, pulsed laser deposition, spectroscopic ellipsometry, Raman spectroscopy

チタン酸リチウム薄膜は，安全性，コスト，サイクル寿命の改善により，リチウムイオンマイクロバッテリやハイブリッドスーパーキャパシタに使用される負極材料としてますます注目を集めている。チタン酸リチウムの化学量論組成と結晶中の各構成元素の占有率の制御は，二次電池の高容量化や高寿命化において重要である。これまでのところ，主に純粋なスピネル相の$Li_4Ti_5O_{12}$（LTO）に研究が集中し，チタン系金属酸化物薄膜の広範な領域はごくわずかしか研究されていない。本研究では，パルスレーザ堆積法（PLD）を用いてLTOと$Li_2O$を交互にアブレーションすることにより，チタニア系マイクロアノード（負極）の組成を広範囲に変化させることに成功した。それらの構造をラマン分光法で(RS)分析し，性能をオペランド分光エリプソメトリー(SE)で解析した結果について報告する。

※1　オペランド解析：分光分析等の非接触手法による動作中の高精度解析。

※2　アブレーション：強いレーザー光を原材料に照射し，分解・昇華させることにより望ましい特性の薄膜を形成する手法。

キーワード
マイクロバッテリー，チタン酸リチウム薄膜，パルスレーザー堆積法，
分光エリプソメトリー，ラマン分光法

## Introduction

The expected growth in the number of sensor nodes and other Internet-of-Things devices in the next decade imposes the development of sustainable micro-power sources, whose manufacturing should preferably be compatible with Silicon processing methods for economic reasons. Titania-based electrodes are one among other alternative to metal Li matching these conditions, the most studied one being the spinel $Li_4Ti_5O_{12}$. The insertion

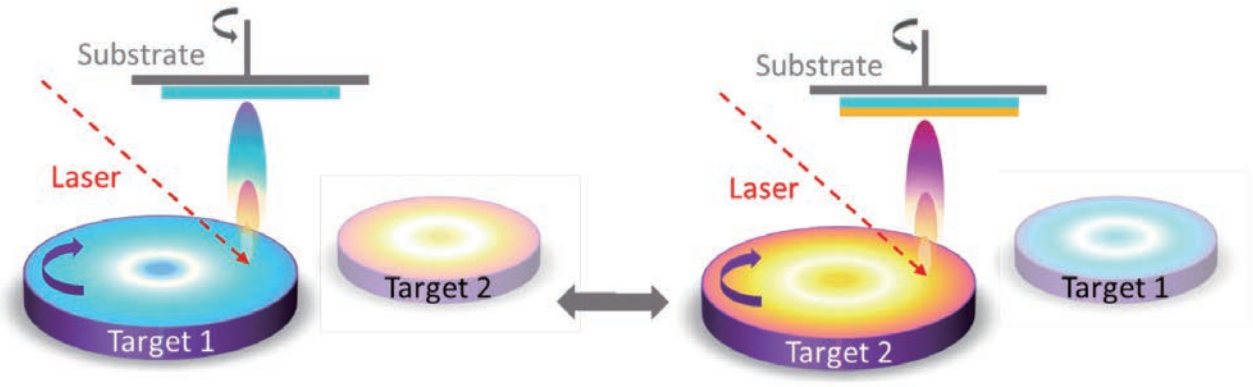


Figure 1 Multi-layer deposition in the PLD. A full cycle is completed after the ablation of each target with a fixed number of pulses. Two targets are alternated repeatedly in cycles until the desired film thickness are reached.

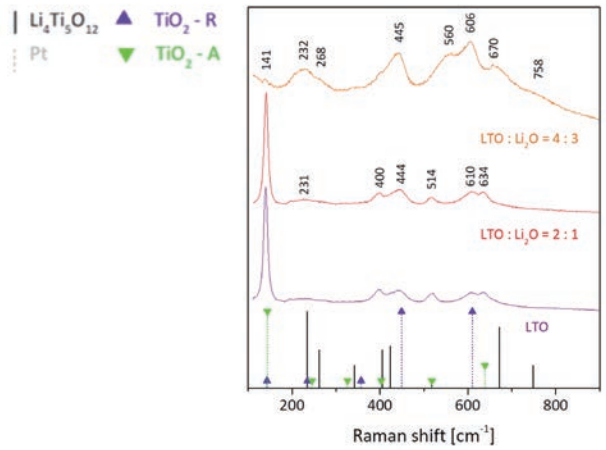


Figure 2 Raman spectra of LTO thin films with different amounts of additional $Li_2O$. Growth conditions are indicated with the deposition pulse ratio LTO : $Li_2O$. Raman references for $TiO_2$ Rutile and Anatase are from literature. [1]

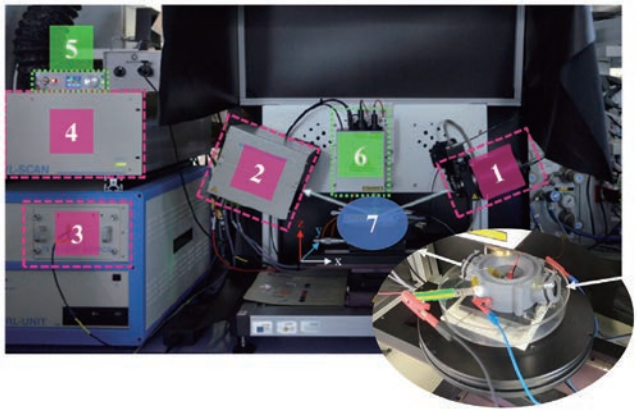


Figure 3 UVISEL (red) and Raman Superhead (green).1: Polarizer, 2: Modulator, 3: Source, 4: Detector, 5: Laser, 6: Raman optics, 7 and insight: electrochemical cell for in operando studies.

of extra lithium into the LTO structure would have a large impact on the accessible capacity of the battery assuming every $Ti^{4+}$ is reduced to $Ti^{3+}$. Typically, LTO is used in the 1.5-3 V range because discharging to 0 V was reported to be unfavorable for the Li-ion diffusion beyond $Li_7Ti_5O_{12}$. Deeper insight about the structural consequences of cycling such alloys to very low potentials is one target of this work.

## Thin film fabrication

The concept of the multi-layer PLD deposition with two different alternating targets is schematically shown in Figure 1.

In this work, the targets were $Li_4Ti_5O_{12}$ and $Li_2O$. Depositions have been carried out on 1cm² Si wafer previously covered with Pt layer to provide electrical accessibility of the anode thin films.

## Analyzing tools, HORIBA Raman SuperHead and UVISEL Spectroscopic Ellipsometer

Raman spectra were collected using a HORIBA Raman SuperHead, coupled to an iHR320 monochromator equipped with a Syncerity CCD detector and a laser at $\lambda$ = 532 nm.

Figure 2 illustrates the Raman spectra of structural evolutions of the $Li_4Ti_5O_{12}$ spinel phase upon a staggered lithium addition. It reveals the main presence of anatase and rutile phases and no evidence of spinel LTO for lower lithium contents. With increasing the $Li_2O$ addition, the anatase signal vanishes and some vibrational modes of LTO become evident. Rutile appears to be present at any lithium concentration, which was confirmed by X-ray diffraction.

Literature has reported that nano-scaled $TiO_2$ shapes have increased the capabilities of lithium uptake for titania-based anodes and promoted their electrochemical

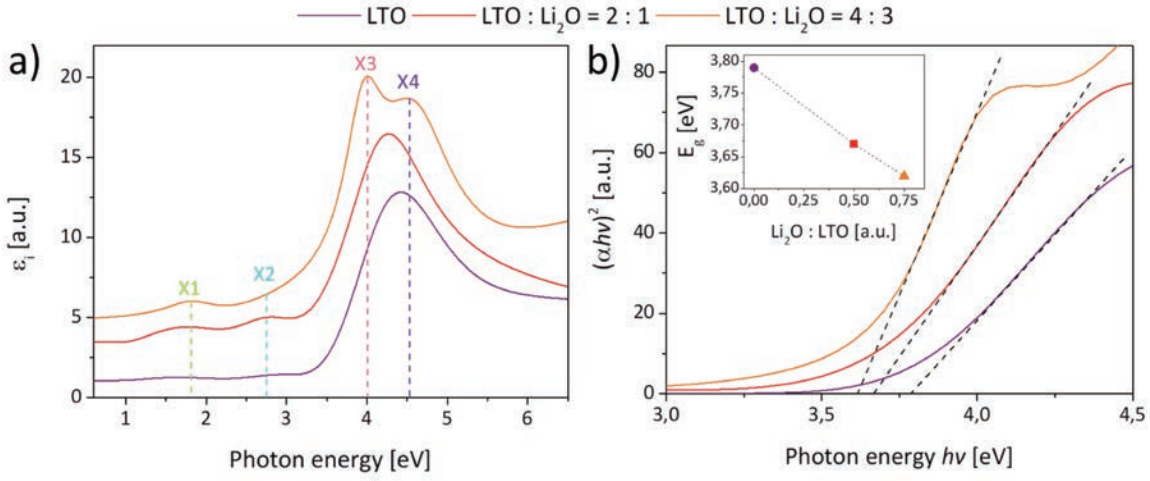


Figure 4 Imaginary part of the permittivity ε for LTO thin films for different LTO : $Li_2O$ ablation ratios in (a). Vertical dashed lines indicate significant changes in absorption bands upon lithium addition, marked and color-coded according to X1 – X4. In (b) the evolution of the band gap for different LTO : $Li_2O$ pulse ratio (as inset) are shown.

activity and performance in batteries[2-5]. While this report is being written, the scanning probe microscope for characterization of such nano objects in operando (HORIBA Electrochemical Tip Enhanced RS) is running first experiments at IREC.

UVISEL phase modulation ellipsometer by HORIBA Scientific was used for optical characterization of the samples. The setup, combined with Raman Superhead is illustrated on Figure 3.

While Raman informs on the structural properties, UV-Visible ellipsometry reveals thickness and optical properties of thin films, the latter corelated to their electrical properties. Figure 4 displays optical properties as imaginary part of dielectric function in a) and bandgap deduced from Tauc plot in b) for LTO with different Li concentrations.

Absorption bands (X1 – X4) occurring in Figure 4 (a) can be attributed to interactions between the electronic states of the $Li_{2s}$ orbital and the hybridized molecule orbitals of $O_{2p}$ and $Ti_{3d}$ forming the $TiO_6$ octahedra[6]. The evolution of these bands is highly correlated to Li diffusion modes through the film and can be controlled by in operando ellipsometry.

Let us first state that a detailed ex situ SE study of the optical properties of LTO:$Li_2O$ composites preceded the operando analysis. It allowed composition analysis by means of usual ellipsometric modeling of effective medium. Then, optical properties for layer evolution during cycling was compared to Figure 4, depending on the $Li_2O$ content and optical absorption bands could be assigned to specific Li ions energetic levels (and corresponding occupancy inside the spinel structure) according to literature. These results set a solid ground for further SE analysis in a dynamic environment.

## Electrochemical performance of the films, discharge to very low potential

The electrochemical experiments have been achieved in 1 M $LiPF_6$ electrolyte and lithium acting as counter and reference electrode in a classic three-electrode setup.

From theory and literature[7,8], the standard reaction potential for the intercalation of three $Li^+$ into spinel $Li_4Ti_5O_{12}$ is known to be 1.5 V vs. Li/Li+ and follows a mechanism expressed in the following equation:

$$Li_{3(8a)}\left(LiTi_5^{4+}\right)_{(16d)}O_{12(32e)} + 3Li_i^+ + 3e^- \rightleftharpoons Li_{6(16c)}\left(LiTi_3^{3+}Ti_2^{4+}\right)_{(16d)}O_{12(32e)}$$

Under continued discharge below 0.6 V vs. $Li/Li^+$, two additional lithium ions can be intercalated at tetrahedral 8a sites in $Li_7Ti_5O_{12}$ by reducing two remaining $Ti^{4+}$ as described in the different following equation:

$$Li_{6(16c)}\left(LiTi_3^{3+}Ti_2^{4+}\right)_{(16d)}O_{12(32e)} + 2Li_i^+ + 2e^- \rightleftharpoons Li_{2(8a)}Li_{6(16c)}\left(LiTi_5^{3+}\right)_{(16d)}O_{12(32e)}$$

Cyclic voltammograms (CV) and chronopotentiometry measurements have been collected at different current densities in the potential range of 0.3 – 3.5 V vs. $Li/Li^+$ and are shown in Figure 5 for different LTO : $Li_2O$ films. For the calculation of specific capacities, the thicknesses determined by SE have been implemented.

Constant current charge and discharge (chronopotentiometry) curves in Figure 5 (b, d, f) exhibit a steady increase in the specific capacities, strongly correlated to the addition of $Li_2O$ during deposition. Excellent charge/discharge profiles are reached with well-defined plateaus for the

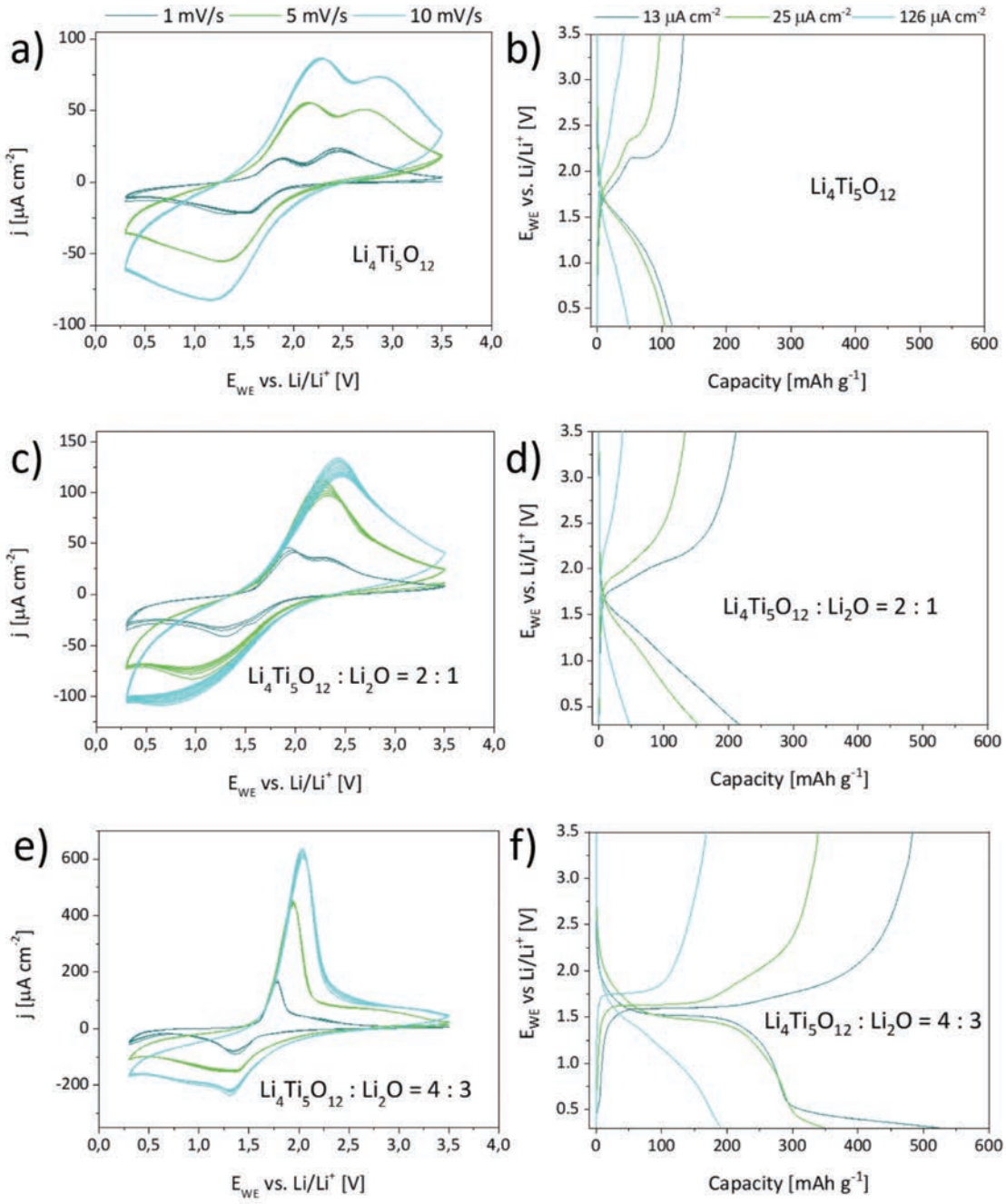


Figure 5 Cyclic voltammograms (left) and constant current charge/discharge curves (right) of LTO layers without additional $Li_2O$ in (a,b) and with additional $Li_2O$ in a pulse ratio of 2:1 (c,d) and 4:3 (e,f) for LTO : $Li_2O$, respectively. The electrochemical window ranges between 0.3 – 3.5 V vs. $Li/Li^+$. The applied current densities are 13 µA cm-2, 25 µA cm-2 and 126 µA cm-2.

$Ti^{3+/4+}$ transition (Figure 5 (f)) under further $Li_2O$ addition, resulting in the extraordinary high specific discharge capacity of 298 mAh $g^{-1}$ at 0.5 V vs. $Li/Li^+$ for the 4:3 ablation ratio. An additional plateau appears to begin below 0.5 V vs. $Li/Li^+$, which may be attributed to the extra lithium uptake described earlier by Yi et al.[9] under the occupation of octahedral 16c and tetrahedral 8a sites.[10].

To obtain further insights about phenomena taking place at these very low potentials, we performed operando SE during the first cycle on a pristine film with high Li-content (LTO: $Li_2O$ ratio of 4:3).

The first output of our SE analysis is the thickness evolution of the lithiated layer with time for the three different regimes (open symbols in Figure 6a referred to the right y-axis). Remarkably, the thickness evolution of the entire film follows quite accurately the shape of the charge injection for the 3 regimes, which indicates a change in volume upon lithiation/de-lithiation. In the imaginary part of the dielectric function, two distinctive features evolving with time are present in all cases, namely, a lower band at ~1.5 eV, and a higher band at ~ 4 eV (Figure 6b).

For regime I, our data are in excellent agreement with

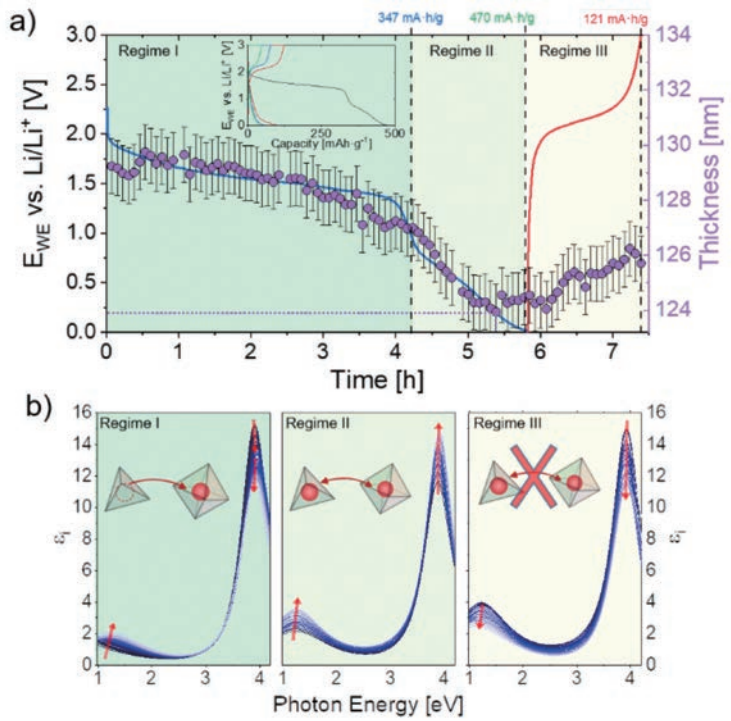


Figure 6 (a) Constant current charge and discharge curves collected under a current density of 3.6 µA cm-2 (0.17 C-rate) monitored by operando SE. The inset shows the charge-discharge profiles of the operando experiment as a function of capacity. Right-axis (purple) shows the thickness evolution of the entire film with time. (b) Optical absorption as a function of the photon energy corresponding to the three different regimes described in the main text (arrows indicate the evolution with time along the experiment). Insets represent the lithium occupancy in the LTO lattice.

previous experimental results and first principle calculations predicting that during lithiation from $Li_4Ti_5O_{12}$ to $Li_7Ti_5O_{12}$, the intensity of the high energy band should decrease while the low energy band should increase [11,12].

Beyond $Li_7Ti_5O_{12}$, i.e., regime II, the lithiation process is far less explored and, to the best of our knowledge, there is no experimental data to compare with. The increase in intensity of Dielectric function can be related to the role of oxygen in this regime upon further lithium insertions[13-18]

Finally, during the charging process (regime III), both energy modes decrease their intensity. In terms of Li occupation, these observations indicate that only the Li inserted in regime II (at the 8a tetrahedral sites) was extracted upon charging, while the Li inserted in regime I (at 16c positions) could not leave the structure.

Overall, our results back up the relevant idea that the cycling range of LTO-based systems can be safely extended until the limit of ~ 0.2 V, which is beyond the typical value of 1V reported in the literature.

## Conclusion

In this work, Pulsed Laser Deposition (PLD) was used by alternating LTO and Li2O ablations to create a widelandscape in the composition of titania-based micro-anodes.

The alternating ablation of LTO and $Li_2O$ targets in the PLD provides a good strategy to fabricate highly performing anodes. Stable cycling was achieved down to potentials of 0.2 V. The structural consequences of cycling in the low potential region during the first discharge were studied using in operando SE. These results provide guidelines to extend the useful cycling range of LTO-based anodes to increase their competitivity versus Li-metal anodes.

## Note

This HORIBA readout contribution is a summarized version of the original paper “Safe extended-range cycling of $Li_4Ti_5O_{12}$-based anodes for ultra-high capacity thin film batteries” published in Materials Today Energy 25 (2022) 10 0979.

* Editorial note: This content in based on HORIBA’s investigation at the year of issue unless otherwise stated.

## References


[1] Lakshmi-Narayana, A.; Hussain, O. M.; Mauger, A.; Julien, C. Transport Properties of Nanostructured $Li_2TiO_3$ Anode Material Synthesized by Hydrothermal *Method. Sci 2019, 1 (39), 1–16.*

[2] Bach, S.; Pereira-ramos, J. P.; Willman, P. Investigation of Lithium Diffusion in Nano-Sized Rutile $TiO_2$ by Impedance Spectroscopy. *Electrochim. Acta 2010, 55 (17), 4952–4959.* *https://doi.org/10.1016/j.electacta.2010.03.101.*

[3] Subramanian, V.; Karki, A.; Gnanasekar, K. I.; Posey, F.; Rambabu, B. Nanocrystalline $TiO_2$ (Anatase) for Li-Ion Batteries. *J. Power Sources 2006, 159, 186–192.* *https://doi.org/10.1016/j.jpowsour.2006.04.027.*

[4] Patil, S. B.; Phattepur, H.; Kishore, B.; Nagaraju, R. V. G. Robust Electrochemistry of Black $TiO_2$ as Stable and High - Rate Negative Electrode for Lithium - Ion Batteries. *Mater. Renew. Sustain. Energy 2019, 8 (2), 1–10.* *https://doi.org/10.1007/s40243-019-0147-y.*

[5] Lindström, H.; Södergren, S.; Solbrand, A.; Rensmo, H.; Hjelm, J.; Hagfeldt, A.; Lindquist, S.-E. Li+ Ion Insertion in $TiO_2$ ( Anatase ). Voltammetry on Nanoporous Films. *J. Phys. Chem. B 1997, 2 (97), 7717–7722.* *https://doi.org/10.1021/jp970490q.*

[6] Liu, Y.; Lian, J.; Sun, Z.; Zhao, M.; Shi, Y.; Song, H. The First-Principles Study for the Novel Optical Properties of $LiTi_2O_4$, $Li_4Ti_5O_{12}$, $Li_2Ti_2O_4$ and $Li_7Ti_5O_{12}$. *Chem. Phys. Lett. 2017, 677, 114–119.* *https://doi.org/10.1016/j.cplett.2017.04.009.*

[7] Ge, H.; Li, N.; Li, D.; Dai, C.; Wang, D. Study on the Theoretical Capacity of Spinel Lithium Titanate Induced by Low-Potential Intercalation. *J. Phys. Chem. C 2009, 113, 6324–6326.*

[8] Raja, M. W.; Mahanty, S.; Kundu, M.; Basu, R. N. Synthesis of Nanocrystalline $Li_4Ti_5O_{12}$ by a Novel Aqueous Combustion Technique. *J. Alloys Compd. 2009, 468, 258–262.* *https://doi.org/10.1016/j.jallcom.2007.12.072.*

[9] Yi, T.-F.; Yang, S.-Y.; Xie, Y. Recent Advances of $Li_4Ti_5O_{12}$ as Promising next Generation Anode Material for High Power Lithium-Ion Batteries. *J. Mater. Chem. A 2015, 3, 5750−5777.* *https://doi.org/10.1039/C4TA06882C.*

[10] Liu, H.; Zhu, Z.; Huang, J.; He, X.; Chen, Y.; Zhang, R.; Lin, R.; Li, Y.; Yu, S.; Xing, X.; Yan, Q.; Li, X.; Frost, M. J.; An, K.; Feng, J.; Kostecki, R.; Xin, H.; Ong, S. P.; Liu, P. Elucidating the Limit of Li Insertion into the Spinel $Li_4Ti_5O_{12}$. *ACS Mater. Lett. 2019, 1 (1), 96–102.* *https://doi.org/10.1021/acsmaterialslett.9b00099.*

[11] Joshi, Y.; Saksena, A.; Hadjixenophontos, E.; Schneider, J. M.; Schmitz, G. Electrochromic Behavior and Phase Transformation in $Li_{4+x}Ti_5O_{12}$ upon Lithium-Ion Deintercalation/Intercalation. *ACS Appl. Mater. Interfaces 2020, 12 (9), 10616–10625.* *https://doi.org/10.1021/acsami.9b19683.*

[12] Liu, Y.; Lian, J.; Sun, Z.; Zhao, M.; Shi, Y.; Song, H. The First-Principles Study for the Novel Optical Properties of $LiTi_2O_4$, $Li_4Ti_5O_{12}$, $Li_2Ti_2O_4$ and $Li_7Ti_5O_{12}$. *Chem. Phys. Lett. 2017, 677, 114–119.* *https://doi.org/10.1016/j.cplett.2017.04.009.*

[13] Borghols, W. J. H.; Wagemaker, M.; Lafont, U.; Kelder, E. M.; Mulder, F. M. Size Effects in the Li4+x$Ti_5O_{12}$ Spinel. *J. Am. Chem. Soc. 2009, 131 (49), 17786–17792.* *https://doi.org/10.1021/ja902423e.*

[14] Zhong, Z.; Ouyang, C.; Shi, S.; Lei, M. Ab Initio Studies on $Li_{4+x}Ti_5O_{12}$ Compounds as Anode Materials for Lithium-Ion Batteries. *ChemPhysChem 2008, 9 (14), 2104–2108.* *https://doi.org/10.1002/cphc.200800333.*

[15] Wang, F.; Wu, L.; Ma, C.; Su, D.; Zhu, Y.; Graetz, J. Excess Lithium Storage and Charge Compensation in Nanoscale $Li_{4+x}Ti_5O_{12}$. *Nanotechnology 2013, 24 (42).* *https://doi.org/10.1088/0957-4484/24/42/424006.*

[16] Kick, M.; Scheurer, C.; Oberhofer, H. Formation and Stability of Small Polarons at the Lithium-Terminated $Li_4Ti_5O_{12}$ (LTO) (111) Surface. *J. Chem. Phys. 2020, 153 (14), 1–9.* *https://doi.org/10.1063/5.0021443.*

[17] Qiu, J.; Lai, C.; Gray, E.; Li, S.; Qiu, S.; Strounina, E.; Sun, C.; Zhao, H.; Zhang, S. Blue Hydrogenated Lithium Titanate as a High-Rate Anode Material for Lithium-Ion Batteries. *J. Mater. Chem. A 2014, 2 (18), 6353–6358.* https://doi.org/10.1039/c4ta00556b.

[18] Jeong, J. H.; Park, B. H.; Lee, G. W.; Roh, K. C.; Kim, K. B. Phase Transformation of Spinel $Li_4Ti_5O_{12}$ to Anatase TiO2 by Catalytic Delithiation. *Energy Storage Mater. 2020, 25 (September 2019), 510–519.* *https://doi.org/10.1016/j.ensm.2019.09.031.*



**Valerie SILLER, Ph. D.**
バレリー シラー
Catalonia Institute for Energy Research (IREC)

**Alex MORATA, Ph. D.**
アレックス モラタ
Catalonia Institute for Energy Research (IREC)

**Juan Carlos Gonzalez-ROSILLO, Ph. D.**
フアン カルロス ゴンサレス ロシリョ
Catalonia Institute for Energy Research (IREC)

**Marc Nuñez EROLES, Ph. D.**
マルク ヌネス エロレス
Catalonia Institute for Energy Research (IREC)

**Michel STCHAKOVSKY, Ph. D.**
ミッシェル スタコフスキー
HORIBA Scientific,
HORIBA FRANCE SAS

**Albert TARANCON, Ph. D.**
アルベルト タランコン
Catalonia Institute for Energy Research (IREC)